Engineering Geology 234 (2018) 11–26

Contents lists available at ScienceDirect

Engineering Geology

journal homepage: www.elsevier.com/locate/enggeo

Assessing the internal structure of landslide dams subject to possible piping erosion by means of microtremor chain array and self-potential surveys

Fawu Wang[a,*], Austin Chukwueloka-Udechukwu Okeke[b], Tetsuya Kogure[a], Tetsuya Sakai[a], Hisao Hayashi[c]

[a] Department of Geoscience, Interdisciplinary Faculty of Science and Engineering, Shimane University, 1060 Nishikawatsu, Matsue, Shimane 690-8504, Japan
[b] Department of Civil Engineering, College of Engineering, Covenant University, Ota, Ogun State, Nigeria
[c] Geo-X Consultants Corporation, Saitama 331-0812, Japan

ARTICLE INFO

Keywords:
Landslide dams
Microtremor chain survey
Self-potential
Phase velocity
Internal structure

ABSTRACT

An integrated geophysical approach comprising microtremor chain array and self-potential surveys was used to assess the internal structure of landslide dams subject to possible piping erosion in selected sites in Japan and Kyrgyzstan. The non-invasive geophysical approach is cost effective, environmentally friendly and portable, and hence, it has proven to be valuable for the geotechnical assessment of landslide dams where piping can trigger failure of the dam. While the microtremor chain array survey results revealed the internal structure of the landslide dam, the self-potential survey results indicated the path of anomalous seepage zones. In the surveyed sites of long-existing landslide dams, the presence of a seepage path in the dam was confirmed by a good correlation between the areas of low phase velocity and large negative self-potential anomalies. In summary, this integrated geophysical approach could be useful for the early risk assessment of landslide dams and prediction of landslide dam failure by piping.

1. Introduction

Landslide dams are common geomorphic features in many mountainous regions of the world (Costa and Schuster, 1988; Evans et al., 2011). These geomorphic hazards are formed where frequent slope movements and fluvial dissection result in high denudation processes that cause valley floor blockages (Korup et al., 2004). Landslide dams are potentially dangerous natural phenomena made up of heterogeneous masses of unconsolidated or poorly consolidated sediments, and thus, they can fail via piping or overtopping (Schuster et al., 1998). The failure of landslide dams could trigger catastrophic outburst floods and debris flows, which could inundate the downstream areas, causing loss of lives and infrastructural damage (King et al., 1989; Becker et al., 2007).

Understanding the predisposing factors and geomorphic processes that lead to the failure of landslide dams is essential for risk assessments. Empirical and statistical methods have been employed in the evaluation of the stability of many landslide dams (Ermini and Casagli, 2003; Korup, 2004; Dong et al., 2009) and potential outflow hydrographs (Evans, 1986; Walder and O'Connor, 1997; Satofuka et al., 2010). However, these methods do not consider the internal structure of landslide dams, and they have been applied to a limited number of datasets (Ermini and Casagli, 2003; Dong et al., 2009). For long-existing landslide dams subject to possible piping and internal erosion, it is important to understand the internal structure of the dam and piping path inside it to carry out failure prediction.

Geophysical investigation can play a crucial role in characterising the internal structure of landslide dams and detecting anomalous seepage at its early stage, which will likely develop into full-scale piping at an early stage. Microtremor (MTM) chain array and self-potential (SP) surveys are two cost-effective (non-invasive) geophysical approaches that can be used to perform detailed on-site assessment of landslide dams' susceptibility to failure by piping and internal erosion. They can be applied on rugged and remote terrains and other hydraulic structures where boring and drilling may be impossible. Similar non-invasive geophysical techniques have been used to identify anomalous seepage in embankment dams (Corwin, 1990; Sjödahl et al., 2005; Moore et al., 2011) and the phase velocity structure of many sedimentary deposits (Apostolidis et al., 2004; Asten et al., 2005; García-Jerez et al., 2008; Sasaki et al., 2015). Fig. 1 shows our concept for measurement and monitoring of landslide dams for failure prediction, especially for those subject to long-term piping and internal erosion. An MTM chain survey is used to detect the internal structure of the landslide dams. For newly formed landslide dams, the results can be used

* Corresponding author.
E-mail address: wangfw@riko.shimane-u.ac.jp (F. Wang).

https://doi.org/10.1016/j.enggeo.2017.12.023
Received 10 December 2016; Received in revised form 25 December 2017; Accepted 27 December 2017
Available online 28 December 2017
0013-7952/

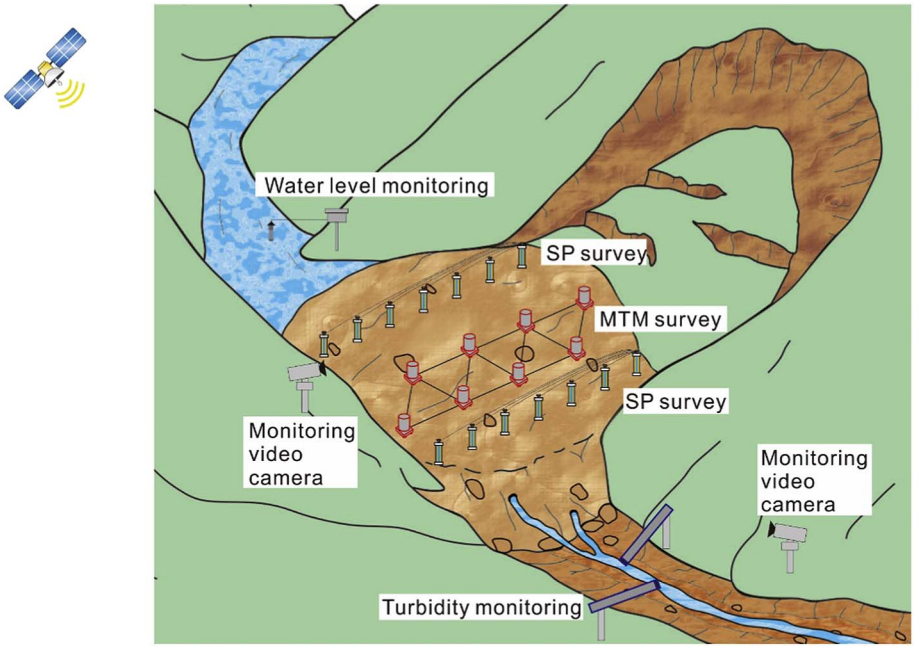

Fig. 1. Concept of measuring and monitoring a landslide dam for failure prediction. A microtremor (MTM) chain array survey is used to detect the internal structure of the landslide dam, and a self-potential (SP) survey is used to detect the location of the groundwater flow path, while the water level on the upstream side and the turbidity on the downstream side are under monitoring. Two video cameras and GPS are used to monitor the surface deformation of the landslide dam.

for the first evaluation of the possible path of piping and internal erosion, while for long-existing landslide dams, the results can be employed to evaluate the internal structure of the dam and check whether and where possible internal erosion has occurred. The SP method can be used for detecting the active water flowing path in a landslide dam.

In this paper, MTM chain array and SP surveys were conducted at several sites in and beyond Japan to estimate the phase velocity structure of landslide dams and obtain information on the likely presence of active seepage zones in the dams. The results could help in assessing the stability of the landslide dams and predicting their potential failure mechanisms, including the time of failure. The frequency of occurrence of landslide dams in Japan has made these geophysical approaches preferable over other methods. The main objectives of this study are as follows: (1) to confirm the applicability of the MTM chain array survey in detecting the internal structure of landslide dams; and (2) to confirm the applicability of SP surveys in identifying potential anomalous seepage zones in a landslide dam and evaluate the likely relationships between these seepage zones and the upstream lake.

2. Methods

2.1. Microtremor chain array survey

An MTM survey is a passive surface wave technique used for measuring natural surface waves. The approach has been used to obtain the shear-wave velocity (V_S) structure and apparent phase velocity depth profiles of geological structures to depths of 100–1000 m (Asten, 2004). Fig. 2 shows the concept of the MTM using the micromotion signals to obtain the phase velocity structure of the ground, employing the dispersion phenomenon of surface waves.

MTMs comprise low-energy body and surface wave motions, which have amplitudes that range from 10^{-4} to 10^{-2} mm (Okada et al., 1990, 2003; Roberts and Asten, 2005). The ordinary MTM method has been applied in the study of the internal structure and dynamic properties of landslide dams and other sedimentary basins (Nakamura, 1989; Ibs-von Seht and Wohlenberg, 1999; Brown et al., 2000; Satoh et al., 2001; Arai and Tokimatsu, 2004; Roberts and Asten, 2005). The results showed that this method has great potential for application in landslide dam investigation. Similarly, the method has been used in the determination of the geometry of sediment deposits and variation of their dynamic properties with depth (Apostolidis et al., 2004, 2006).

Two methods commonly used for processing MTM data are the frequency (f) – wavenumber (k) power spectral density (FK) method (Capon, 1969; Lacoss et al., 1969) and the spatial autocorrelation (SAC) method (Aki, 1957, 1965; Okada, 2003). The most commonly used array for SAC measurements is the circularity array, which can be substituted with the semi-circularity array (Okada, 2003). The SAC measurement method has been developed as the extended SAC (ESAC) approach by Ling and Okada (1993) and Okada (1994). With this improvement, the array configuration can be arbitrarily shaped, and the Rayleigh wave phase velocity can be as accurate as those obtained using the FK method (Ohori et al., 2002).

Fig. 3 shows the abstracting method of the dispersion curve, that is, the relationship between the frequency and phase velocity, from micromotion signals monitored with MTM sensors, namely seismometers (Hayashi et al., 2010). The micromotion signals are recorded simultaneously by the MTM sensor located at the centre and lots of MTM sensors located at the circle, which are quidistant from the circle centre. This is called a circularity array.

Using the following procedure, the dispersion curves can be obtained:

1) Calculate the wave-shape correlation $r_{xy}(f,\theta,r)$ between the circle centre and each sensor point at the periphery using the complex coherence function (Fig. 3a):

$$r_{xy}(f,\theta,r) = \frac{R_e[S_{xy}(f,\theta,r)]}{\sqrt{S_x(f)\cdot S_y(f,\theta,r)}} \quad (1)$$

where R_e denotes the real part of the complex function $S_{xy}(f,\theta,r)$, f is the frequency, θ is the angle at the periphery, and r is the radius of the circle.

2) Use the property wherein the average value of the spatial autocorrelation coefficient is equal to the value of the Bessel function (Fig. 3b) and obtain the SAC coefficient:

$$\rho(f) = \frac{1}{2\pi}\int_0^{2\pi} r_{xy}(f,\theta,r)d\theta = J_0\left(2\pi f\frac{r}{c(f)}\right) \quad (2)$$

where $\rho(f)$ is the SAC coefficient, J_0 is the 0 order of the first-sort Bessel function, and $c(f)$ is the phase velocity.

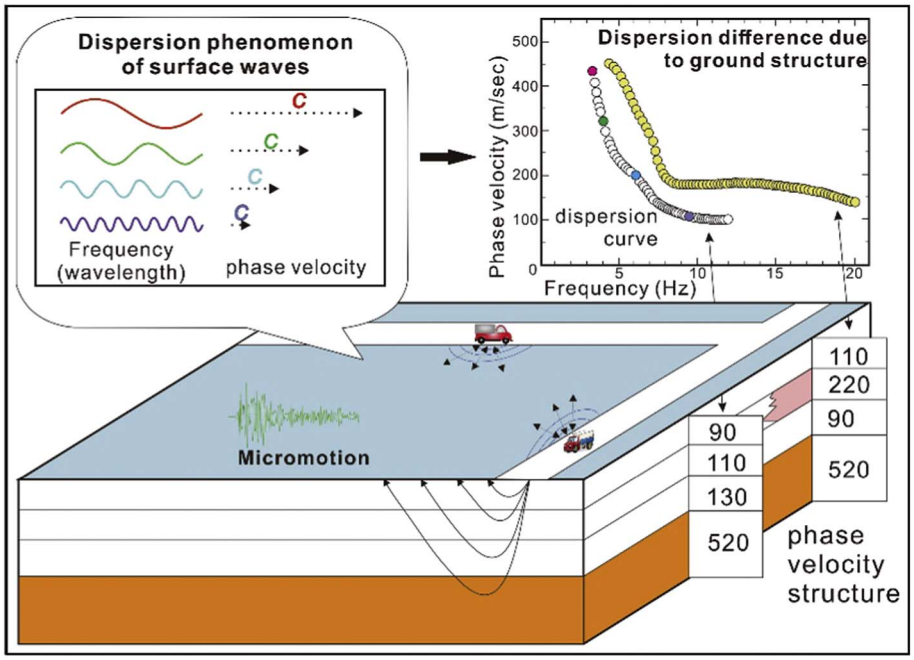

Fig. 2. Concept of a microtremor (MTM) survey using the micromotion signals to obtain the phase velocity structure of a ground, employing the dispersion phenomenon of surface waves (modified from Hayashi et al., 2010).

3) Obtain the phase velocity from the inverse function of the Bessel function (Fig. 3c):

$$c(f) = 2\pi f \frac{r}{J_0^{-1}(\rho(f))} \tag{3}$$

where $J_0{}^{-1}$ is the inverse of the J_0 function.

According to Okada (2001, 2006), to abstract the dispersion curve, at least three MTM sensors should be located at the periphery. Fig. 4 shows two examples of the array method using the SAC approach. One example is an equilateral triangle array, and the other is a multiple array. A multiple array is much better than an equilateral triangle array, as it can cover a wider range of wavelengths. The wavelength of the surface wave in the dispersion wave reflects the situation at a depth of 1/2 to 1/3 of the wavelength. As shown in Fig. 5, based on this principle, the phase velocity structure can be obtained via conversion from the curve between frequency and depth (Hayashi et al., 2010).

Using the semi-circularity array, Okada et al. (2003) developed a new array called the MTM chain array. This method makes it possible to obtain a two-dimensional underground phase velocity structure model via continuous measurement (Hayashi et al., 2010). Due to this advantage, this method was selected in the present study for application to landslide dams. Fig. 6a shows the principle of transferring the circularity array to a semi-circularity array, and finally, the MTM chain array. Through the data obtained from seismometers 1, 2, 3 and 4, the average phase velocity around seismometer 1 can be obtained via an analysis using the SAC method. With the MTM chain array, as shown in Fig. 6b, the average phase velocity under seismometers 3, 5, 7 and 9 can be measured simultaneously. When using 11 seismometers, seismometers 1 and 2 will be set at the current positions of seismometers 10 and 11, followed by the other seismometers, and then the second-round measurement can be conducted. Ultimately, a continuous, two-dimensional phase velocity–depth profile can be obtained. Fig. 6c shows an example of the layout of 12 seismometers on an irrigation dam top to confirm the effectiveness of the MTM chain array survey.

Generally, an MTM survey can give the S-wave velocity structure as the result via modelling based on the dispersion relationship between the frequency and wavenumber. However, to maintain the original continuity and discontinuity of the measured area, only minimum processing is carried out on the measured data to keep the anomalies, and the phase velocity, rather than the shear wave velocity, is presented as the result in the MTM chain array method (Hayashi et al., 2010). Like shear wave velocities, Rayleigh wave phase velocities depend on the dynamic properties of the soil, such as the density, Poisson's ratio and compression wave velocity (Brown et al., 2000).

In an MTM survey, the effective investigation depth depends on the maximum wavelength that has been measured. It is always hoped that a greater investigation depth can be reached with a smaller array size, which is the lateral length of an equilateral triangle. Matsuoka et al. (1996) examined the relationship between the seismometers (d, corresponding to the array size in chain array) and maximum detected wavelength (L). By relating d to L, they obtained a result of L ranging from 30 to 5000 m, corresponding to d ranging from 3 to 150 m. In their study, they also presented the ratio of the maximum wavelength (L) to seismometer spacing (d). The average value of the ratio was 22. When the seismometer spacing was smaller than 30 m and the target ground was soft, the ratio was smaller than average, and it was sometimes less than 10. For ensuring the measurement quality, Matsuoka et al. (1996) proposed that the seismometer spacing d can be set as 1/10 to 1/20 of the expected maximum wavelength. Following this research, Hayashi et al. (2010) proposed that the investigation depth can be 10 times the array size when applying this method for geotechnical purposes. Matsuoka et al. (1996) also examined the necessary measuring time in the SAC method. They concluded that, for array sizes of 3–30 m, the time should be 10 min, while for an array size of 60 m, the time should be 20 min (Hayashi et al., 2010).

For our purpose of detecting the internal structure of landslide dams, the array size of the equilateral triangles was fixed at 1.5–10 m, depending on the depth of investigation and desired range of Rayleigh wave wavelengths. Also, the time duration for each measurement ranged from 15 to 30 min.

For data processing, Matsuoka et al. (1996) developed a method of drawing the dispersion curves of surface waves, which made it possible to obtain the relationship between the phase velocity and depth. Using the MTM data recorded by the seismometers located at the circularity array and centre simultaneously, the correlation between the centre point and the points on the circle can first be calculated, and then the SAC coefficient, that is, the $\rho(f)$ curve, can be obtained. Fig. 7 shows an example of a $\rho(f)$ curve. Following this, through an inverse operation, the dispersion curves (Fig. 8), that is, the relationship between the

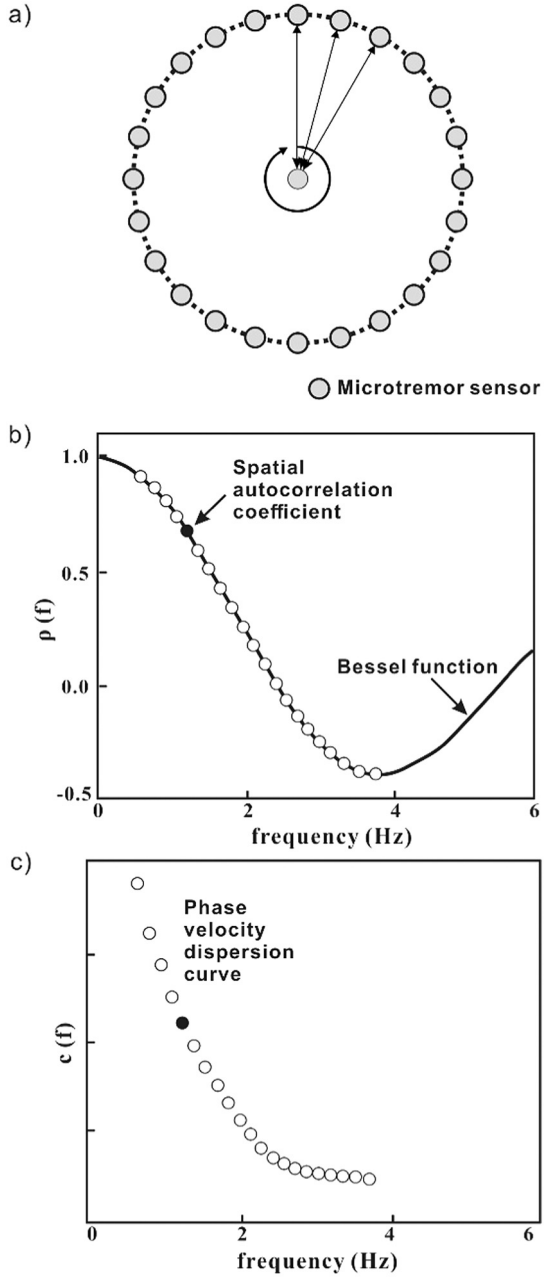

Fig. 3. Procedure for obtaining the dispersion curve by means of the spatial autocorrelation (SAC) method: a) circularity array to calculate the correlation between the central point and the point at the periphery, b) using the Bessel function to obtain the SAC coefficient, c) obtaining the phase velocity from the inverse function of the Bessel function (modified from Hayashi et al., 2010).

phase velocity and frequency, can be obtained.

The GX-GS01 seismometer used in this study is a velocity seismometer with a natural period of 1.0 s. The coil resistance is larger than 10 kΩ, and the sensitivity is greater than 5 V/kine. During the measurement, the seismometer was set on a GX-SP01 horizontal iron plate of 200 ∗ 200 mm (length ∗ width), which has a pin of 200 mm in length and can be fixed into the ground.

The GX-LG01 amplifier has 12 channels and three sampling rates, that is, 50 Hz, 100 Hz and 200 Hz. There are two types of low-pass filter, that is, 1 Hz and 30 Hz. During the measurement, the results are shown on a laptop screen in real time. In this study, a sampling rate of 100 Hz and low-pass filter of 1 Hz were adopted. The GX-CB01 cable, which can protect against the effect of electromagnetic induction, was used to connect the seismometer and amplifier.

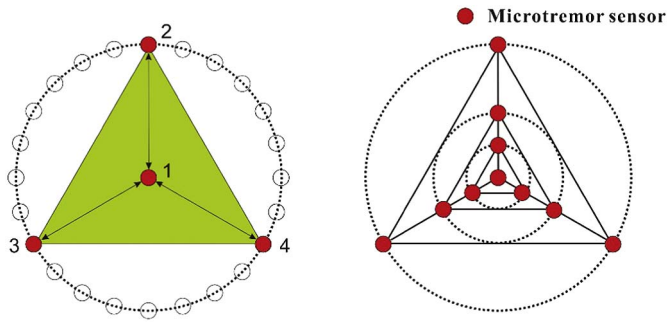

Fig. 4. Two settings of microtremor (MTM) sensors in the spatial autocorrelation (SAC) method. Left: equilateral triangle array; right: multiple array (modified from Hayashi et al., 2010).

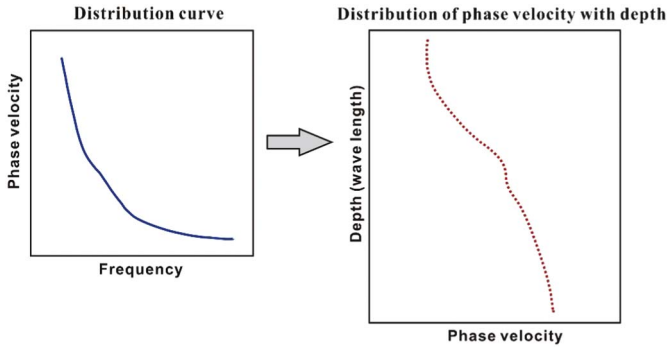

Fig. 5. Transforming procedure from the dispersion curve (left) to phase velocity distribution along the depth (right) (modified from Hayashi et al., 2010).

2.2. The self-potential survey

Landslide dams are generally composed of unconsolidated or disturbed materials, which have no filter zones or engineered water barriers to prevent seepage, and hence, may allow the development of seepage and internal erosion from landslide lakes in front of a landslide dam. To monitor the internal seepage in a landslide dam, the SP method was selected in this study due to its possible response to subsurface fluid paths through the mechanism of the streaming potential. The streaming potential is an electrokinetic process that describes the interaction between the subsurface fluid path and electric flow in a porous rock mass or saturated soil (Glover et al., 2012; Jouniaux and Ishido, 2012). In a saturated system under static conditions, equilibrium exists due to a balance of the electric charge across the solid–fluid interface. The streaming potential evolves from hydraulic action, which offsets the equilibrium of the system, giving rise to a charge imbalance that generates electric currents (Ishido et al., 1983). The electrokinetic process takes place in the pore spaces of saturated soils under constant hydraulic flow. It involves the exchange of charged ions in the pore spaces, and thus, initiates an electric current field, also referred to as the streaming current (Fig. 9a). In natural conditions, the occurrence of streaming potentials results from the double layer of ions associated with the interaction between the mineral grains and pore-water (Allegre et al., 2010).

The SP method is a passive geophysical technique that responds to naturally occurring potentials on the earth's surface. It is unique in its ability to detect natural or ‘spontaneous’ voltages on the ground generated by hydraulic, thermal and chemical processes. An SP survey is useful for locating and quantifying groundwater flows and pollutant plume spreading, as well as estimating the pertinent hydraulic properties of aquifers (water table, hydraulic conductivity). This method has been employed in embankment dam engineering for the delineation of anomalous zones that correspond to preferential seepage paths (Corwin, 1991). In addition, in recent years, the technique has been

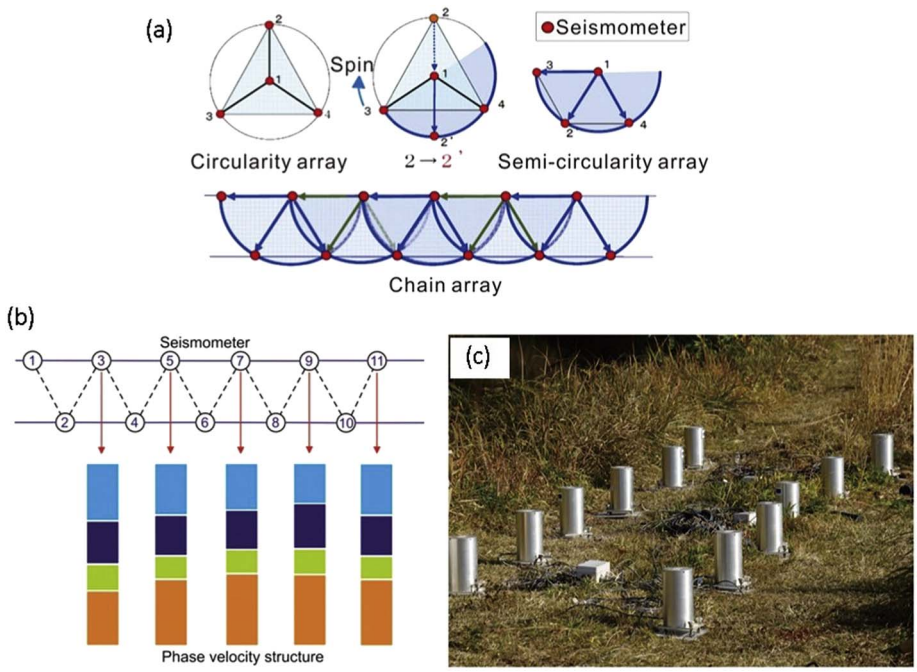

Fig. 6. Microtremor (MTM) chain array survey: a) Principle of the MTM chain array method based on circularity arrays of seismometers. Moving no. 2 to no. 2′, the circularity array becomes a semi-circularity array. Rotating line 3–1 to a horizontal line and adding more MTM sensors paralleling line 1–4, a chain array is formed (from Hayashi et al., 2010). b) Determination of the phase velocity depth profile using the chain array (modified from Hayashi et al., 2010). c) Photo of the seismometers in the chain array.

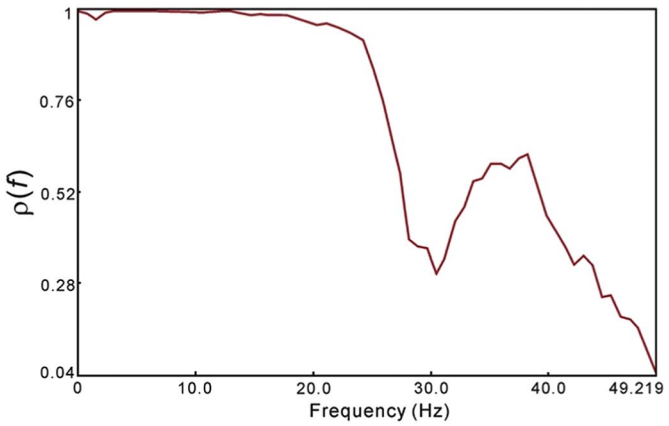

Fig. 7. Example of a spatial autocorrelation (SAC) coefficient curve.

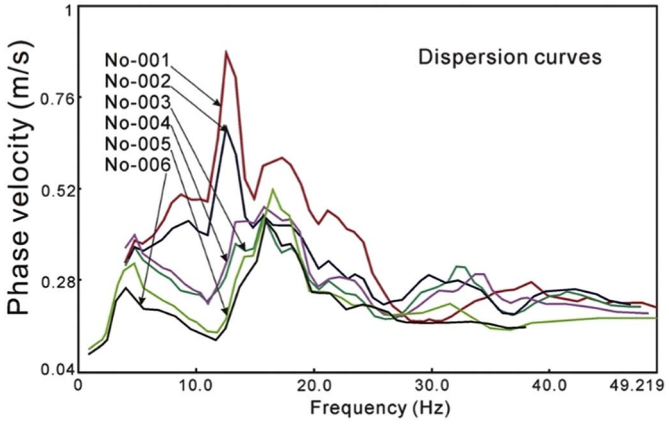

Fig. 8. Examples of dispersion curves for six seismometers in a survey.

applied for monitoring seepage, internal erosion and piping in landslide dams and natural and engineered levees (Bolève et al., 2009; Moore et al., 2011; Thompson et al., 2012).

SP surveys were taken using two methods, namely the leapfrog method and fixed-base method. The leapfrog method, also called the gradient method or dipole method, measures the potential between two electrodes, and the two electrodes are leapfrogged along the measure line (Fig. 9b). The advantage of this method is that two electrodes are sufficient to conduct the measurement. The fixed-base method, also called the total field method, measures the potential difference between a fixed-base electrode and a mobile electrode connected to a long reel of wire (Fig. 9c). This approach has the advantage of flexibility in placing the mobile electrode, and it usually gives a smaller cumulative error than the leapfrog method does (Lowrie, 2007). Fig. 9d shows the image of the result curves with the two methods. When a measure line passes over a groundwater flowing route, the result curve appears as an S-shape when the leapfrog method is used, while it appears as a wide V-shape when the fixed-base method is used. In this study, the fixed-base method was employed for all measurements.

Non-polarising copper/copper sulphate electrodes (model no.: RE-5; diameter, 0.035 m, length, 0.15 m; Nippon Corrosion Engineering Co., Ltd) were used in this study. At each station, a small amount of salted bentonite mud was added to a pre-dug shallow hole for enhancing the coupling between the electrode and ground, especially in dry terrain covered by gravelly deposits. SP surveys were taken using a digital multimeter, M-6000M (METEX), which exhibits a high sensitivity and high input impedance.

3. Site description

In this study, Miyoshi Irrigation Dam was selected to confirm the applicability of the MTM chain array survey (Fig. 10). Then, the MTM chain array survey and SP surveys were conducted in Akatani landslide dam and Kuridaira landslide dam, located in Nara Prefecture, Japan; Terano landslide dam, located in Niigata Prefecture, Japan (Fig. 10); and Kol-Tor landslide dam near Bishkek, Kyrgyzstan Republic (Fig. 11).

3.1. Miyoshi irrigation dam, Japan

The Miyoshi dam is a small irrigation dam located near the Miyoshi highway interchange in Miyoshi City, Hiroshima Prefecture, Japan (Fig. 12). The dam height, length and crest width are about 18 m, 66 m and 1.5 m, while the maximum dam width and downstream slope angle are 66 m and 35–40°, respectively. Fig. 13 shows the front view of the

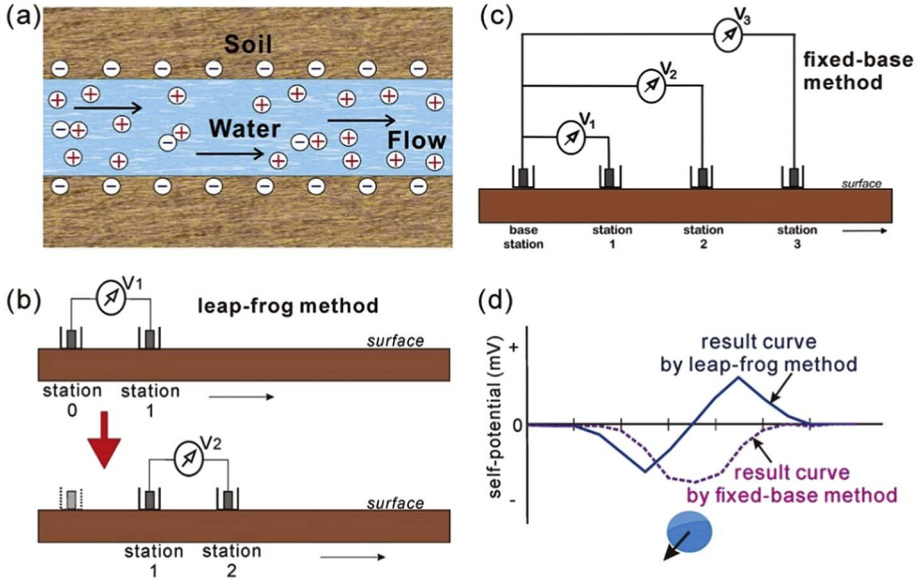

Fig. 9. Principle of the self-potential (SP) measurement for detecting groundwater flowing: a) Schematic diagram of streaming potential in the pore space of a saturated soil. Cations are brought away by the water flow to the downstream side, resulting in a negative SP at the water flow path and positive SP at the downstream side. b) Measurement using the leapfrog method. c) Measurement using the fixed-base method (Lowrie, 2007). d) Images of the result curves of the two methods with a measure line passing over a groundwater flow route.

dam and the location of the measure line A–A′ for the MTM chain array survey. The dam was specifically constructed for the supply of water to several agricultural terraces in the downstream area 20 years ago. It impounds a lake with an estimated volume of 220,000 m^3. There is a drainage pipe (sluiceway) of approximately 0.3 m in diameter located ~5 m below the dam crest. The projection distance from the drainage pipe to the measurement start-point A is 42 m. In addition, excess water from the upstream lake flows into the downstream area through an uncontrolled spillway channel. The distance from the centre of the spillway to the measurement start-point A is 50 m. The structure of the artificial dam laying on the natural valley is obvious. The MTM chain array survey was conducted on the dam from point A to A′ with a total length of 66 m to detect the internal structure of the dam and determine the applicability of the technique for evaluating the internal structure of landslide dams.

3.2. Akatani and Kuridaira landslide dams, Japan

The Akatani and Kuridaira landslide dams are situated in Nara Prefecture on Japan's Kii Peninsula (Fig. 14). The two landslide dams are among the 17 major landslide dams created due to the devastating effects of Typhoon Talas (Typhoon No. 12 in Japan), which occurred between 31 August and 4 September 2011 (Hayashi et al., 2013). The passage of this severe tropical cyclone over the Japanese archipelago brought cumulative precipitation of 1000–1500 mm in the southern part of the Kii Peninsula and 1800–2400 mm over 5 days in some districts of Nara Prefecture. As many as 207 landslides, landslide dams, debris flows and other sediment-related disasters arose in 21 prefectures, with the Mie, Nara and Wakayama Prefectures recording the highest numbers of cases (Sakurai et al., 2016). A summary of the geomorphic characteristics of the two landslide dams is given in Table 1. The sediments composing the landslide dams were derived from the Cretaceous to Paleogene Shimanto accretionary complex, which comprises weathered layers of sandstone, chert, tuff, greenstone, siltstone and foliated mudstone, as well as detached blocks of intrusive rocks. Emergency countermeasure works, including the installation of drainage pumps, subsurface drainage systems and real-time monitoring sensors, have been carried out on the sites to stabilise the landslide dams and prevent the potential occurrence of flood disasters (SABO, 2012). Our measurement was conducted on the engineered landslide dams in August 2012, 1 year after the landslide dams were formed.

3.3. Terano landslide dam, Japan

The landslide dam in Terano district, hereafter referred to as the Terano landslide dam, is located in the Imogawa River basin, Niigata Prefecture, northeast Japan (Fig. 15). The landslide dam was formed by a landslide triggered by the 23 October 2004 M_W 6.8 earthquake, which struck Niigata Prefecture. This earthquake triggered about 1419 shallow landslides and 75 deep-seated landslides near the epicentre (Nagai et al., 2008). Detailed on-site preliminary surveys indicated that 362 of the landslides had a width greater than 50 m, while 12 had a volume greater than 1×10^6 m^3 (Sassa, 2005). Large amounts of materials displaced by this earthquake formed landslide dams at 45 locations on the Imogawa River. Among these, the landslide dams formed by the Terano and Higashi Takezawa landslides had a height of more than 25 m (Sassa, 2005). Most of the sediments forming the landslide dams were derived from poorly indurated and structurally deformed Neogene-Quaternary sedimentary deposits, which comprise mudstone and alternating units of sandstone and mudstone, including conglomerates. The maximum length and volume of the Terano landslide dam are 300 m and 1×10^6 m^3, respectively. Numerous countermeasure works have been carried out on the landslide dam to increase its stability and avert the potential overflow of the upstream lake. Our measurement was conducted in July 2014, 10 years after the landslide dam was formed. At this point, all countermeasure works to stabilise the landslide dam had been completed.

3.4. Kol-Tor landslide dam, Kyrgyzstan

The landslide dam behind Kol-Tor Lake in Kegeti Gorge (hereinafter called the Kol-Tor landslide dam) is located about 90 km southeast of Bishkek, the capital of the Kyrgyzstan Republic. The dam was formed by a rock avalanche that originated from the valley side and blocked the valley floor (Fig. 12). The landslide dam and upstream lake are located at altitudes of 2400–2735 m and 2726 m, respectively, while the lake volume, maximum depth and total surface area are 1.83×10^6 m^3, 14.8 m and 2.215×10^5 m^2, respectively (Fig. 16a; Janský et al., 2010). Even now, it is not clear when the landslide dam was formed. It is estimated that it may have existed for hundreds of years. We carried out the measurement in September 2015. The length, width and thickness of the dam were 1800, 600, and ~25 m, respectively. According to Janský et al. (2010), the lake impounded by the landslide dam was initially formed by a moraine dam. Subsequent rock avalanche processes caused further blockage of the stream channel and led to an

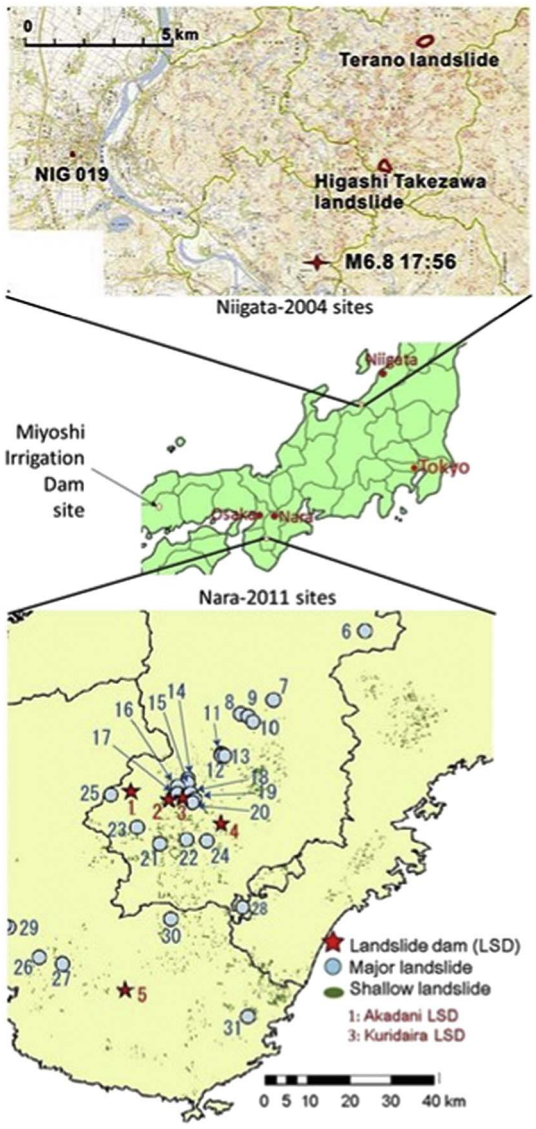

Fig. 10. Location map of the investigation sites in Japan. Akatani landslide dam and Kuridaira landslide dam in Nara Prefecture and Terano landslide dam in Niigata Prefecture were investigated.

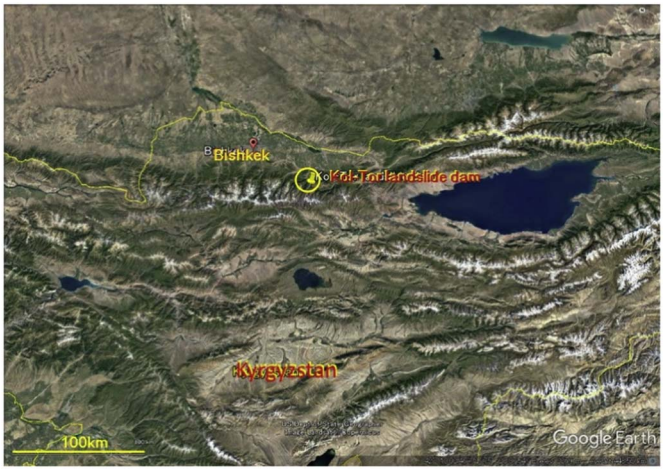

Fig. 11. Location of the Kol-Tor landslide dam in the Kyrgyzstan Republic.

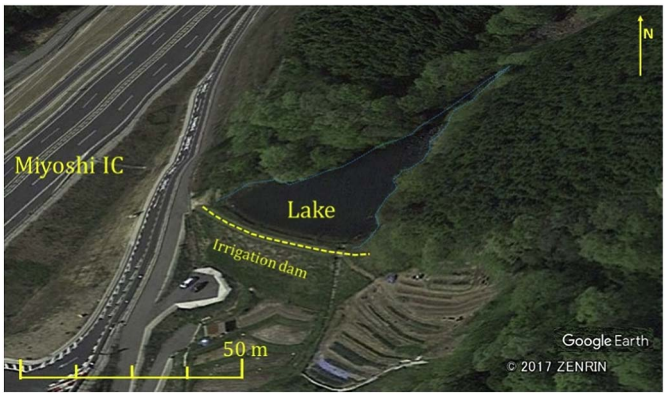

Fig. 12. Location of the Miyoshi Irrigation Dam on a Google Earth image.

increase in height of the dam and depth of the upstream lake. The lower part of the dam comprises moderately consolidated glaciogenic sediments from the underlying moraine deposits, while the upper part comprises poorly sorted clastic sediments, including gravel and boulders. The lake is mostly recharged by snowmelt, rainfall, water from glaciers and subsurface springs. The existence of many subsurface cavities at the downstream end of the dam has been attributed to the effects of the melting glaciers, coupled with incessant precipitations that have led to a steady rise in the upstream lake. In our field investigations in August 2009 and September 2015, rapid seepages were observed (Fig. 16b). Geophysical investigations were carried out on the landslide dam to evaluate the internal structure at the lowest part and try to find the distribution of the SP after long-term seeping under the landslide dam.

4. Results and discussion

4.1. Miyoshi irrigation dam, Japan

The MTM chain array survey was performed along a survey line on the Miyoshi Irrigation Dam crest. The array size was fixed at 2.0 m, while the duration of each measurement was fixed at 30 min.

Fig. 17 shows the phase velocity profile along the dam crest. The measure line on the dam crest started from the right bank of the dam and terminated at the left bank, continuing for 66 m, as shown in Fig. 13. The phase velocity of the dam materials varied from 100 to 900 m/s. The geometry of the dam site can be delineated by the high phase velocity of 540–900 m/s characteristic of the right abutment. The uppermost layers of the dam exhibited low phase velocity that ranged from 100 to 140 m/s, which may indicate the poor or moderately consolidated nature of the refilled materials. Furthermore, the phase velocity ranging from 100 to 120 m/s corresponded to the depth where the drainage pipe was located, which is indicated with a dotted circle. The area around the spillway also showed a low phase velocity zone, which may indicate the effect of the overflow in the spillway on the dam structure. The results of this preliminary investigation demonstrated the reliability of the MTM chain array method in the evaluation of landslide dams' internal structures.

4.2. Akatani and Kuridaira landslide dams

The MTM chain array survey and SP survey were carried out at several locations at the Akatani and Kuridaira landslide dams (Fig. 18). The survey lines were chosen based on the terrain conditions. In total, four MTM chain array survey lines (A–A′, B–B′, C–C′ and D–D′) and three SP survey lines (a–a′, b–b′ and c–c′) were traversed at the Akatani landslide dam, while one MTM survey line (A–A′) and two SP survey lines (a–a′ and b–b′) were covered at the Kuridaira landslide dam (Fig. 19). The array size for the D–D′ line at the Akatani landslide dam

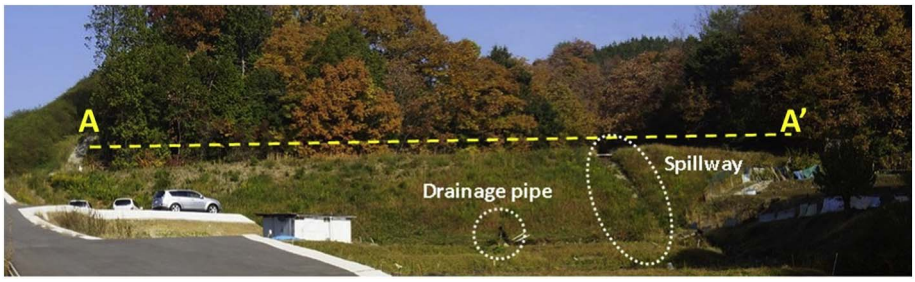

Fig. 13. Front view of the Miyoshi Irrigation Dam and the microtremor (MTM) chain array measure line A–A′ on the dam. The locations of a spillway and drainage pipe are shown.

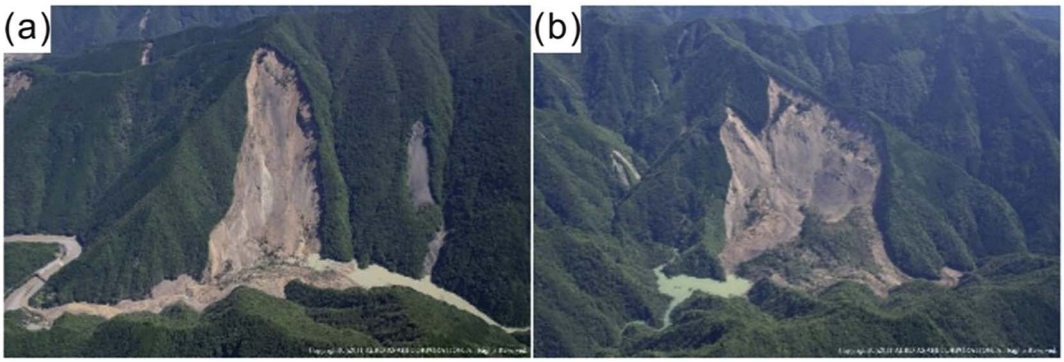

Fig. 14. Two landslide dams triggered by a heavy rainfall in Nara Prefecture, Japan: (a) Akatani landslide dam, (b) Kuridaira landslide dam (Image: Aero Asahi Corp.).

Table 1
Geomorphic characteristics of the Akatani and Kuridaira landslide dams.

Landslide				Landslide dam			
Area	Length (m)	Width (m)	Volume (10^6 m^3)	Height (m)	Blockage volume (10^6 m^3)	Lake volume (10^6 m^3)	Catchment area (km^2)
Akatani	670	300	9.4	67	10.2	5.5	13.2
Kuridaira	600	500	25.1	100	24.1	7.5	8.7

Fig. 15. Front view of the Terano landslide that occurred in 2004 in Niigata Prefecture, Japan (taken in 2014 by F.W. Wang).

was fixed at 1.5 m, while for the other lines at the Akatani and Kuridaira landslide dams, the array size was fixed at 3.0 m. The duration for each measurement of all lines was fixed at 30 min. In all the SP survey lines, the spacing distance between two neighbouring SP stations was fixed at 3 m. Fig. 20 shows the phase velocity profiles along the surveyed lines at the Akatani landslide dam. In general, low phase velocities of 100 to 300 m/s (in blue) were obtained at the survey lines located near the landslide lake (lines B–B′, C–C′ and D–D′). These low phase velocity values can be attributed to the following: (1) the effect of an artificial drainage pipe (at line D–D′) laid inside the dam for lowering the upstream lake (Fig. 21) and (2) the uppermost layer of the sediments, which were made up of poorly consolidated debris from the distal end of the landslide. In contrast, phase velocity ranges of 400–780 m/s were obtained near the central part of the dam (line A–A′). The observed increase in phase velocity with depth resulted from an increase in density and decrease in porosity, from the unconsolidated upper deposits to the bedrock.

Fig. 22 shows the SP profiles along lines a–a′, b–b′ and c–c′ at the Akatani landslide dam. In the three measure lines, all the base stations were put in relatively high and dry positions. Along a–a′, there is almost no negative SP, while most of the area showed a negative SP at line b–b′, and all of line c–c′ showed negative values. The results exhibited marked variations in the SP profiles from the middle of the landslide dam toward the upstream side, and this may imply the absence of well-developed seepage paths in the dam. Attributing SP anomalies to the streaming potential, water infiltration should be expected to flow from zones of negative anomalies to zones of positive ones (cf. Moore et al., 2011), which can reveal whether seepage phenomena occur from the upstream lake through the landslide dam. The high hydraulic conductivity of the poorly consolidated sediments dominating the upper layer of the area near the upstream side may have given rise to the negative SP anomalies of several tens of 20–25 mV.

Integrating the findings in Figs. 21 and 22, some results can be clarified. Lines A–A′ and a–a′ were set at the same line. Perhaps due to the 1-year-old landslide dam, the internal structure on the downstream side of the landslide dam was in a nearly homogenous state, and the SP

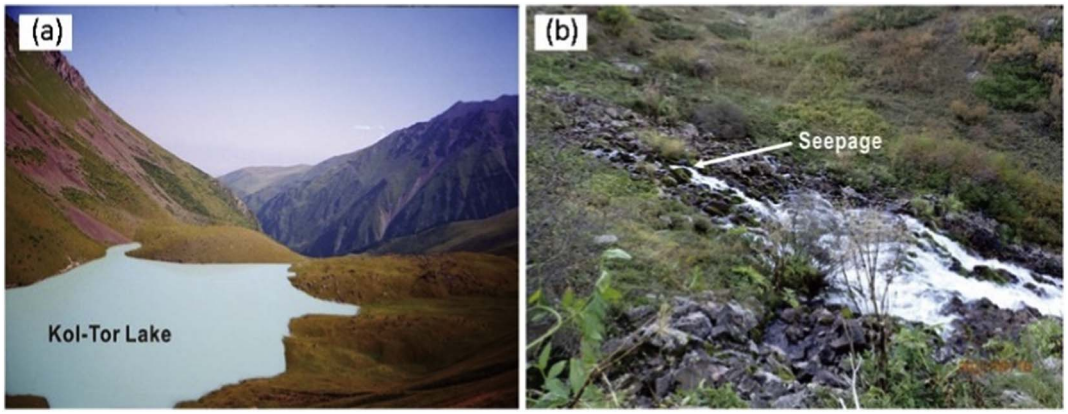

Fig. 16. Situation of the Kol-Tor landslide dam in the Kyrgyzstan Republic: a) Upstream lake impounded by the Kol-Tor landslide dam, b) seepage/spring at the downstream area from the dam (taken in 2009 by F.W. Wang).

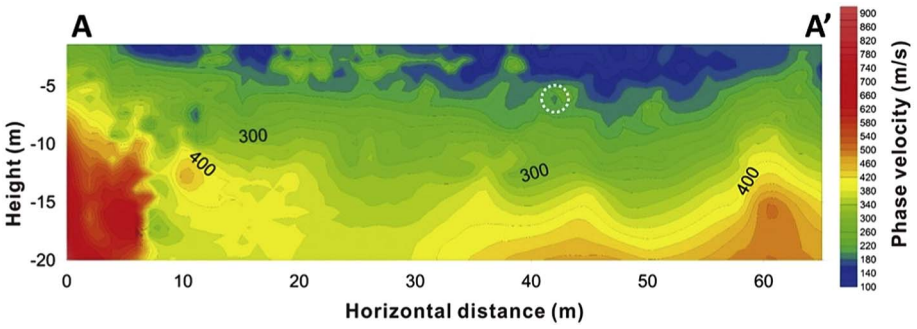

Fig. 17. Phase velocity versus depth profile of the Miyoshi Irrigation Dam obtained with a microtremor (MTM) chain array with an array size of 2.0 m. The location of the drainage pipe is indicated with a dotted circle.

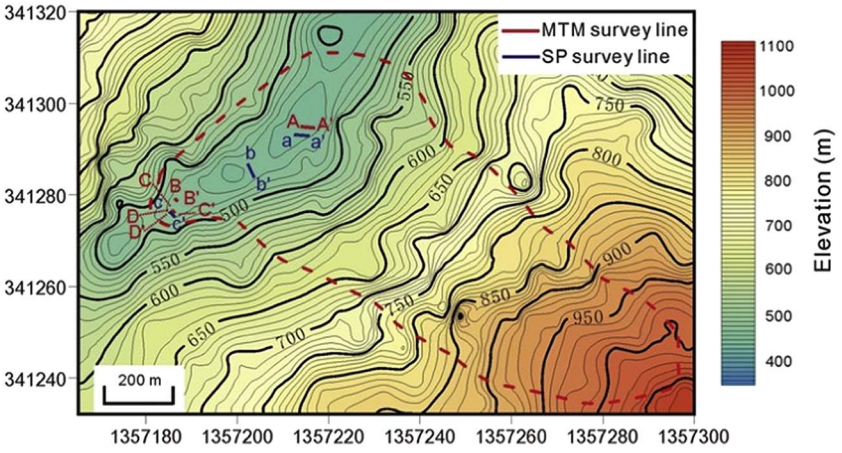

Fig. 18. Site map of the Akatani landslide dam indicating the survey lines for the microtremor (MTM) chain array and self-potential (SP) measurements. The dotted line indicates the boundary of the Akatani landslide.

values were almost all positive. Lines C–C′ and c–c′ started from the same position, but line C–C′ continued for only 13 m, while line c–c′ continued for 31 m. In the line C–C′, between 7 m and 13 m, a loose structure is evident, like a big hole. Corresponding to the loose structure, the SP value along c–c′ presents negative values at all points, with the lowest part between 4 m and 10 m.

Fig. 23 shows the phase velocity depth profile of survey line A–A′ at the Kuridaira landslide dam along the buried valley. The phase velocity distribution of the area varied from 300 to 680 m/s. From the results, the internal structure of the underlying sediment could be divided into three distinct layers. The uppermost layer had phase velocities ranging from 300 to 340 m/s. This layer graded into a sublayer with phase velocities varying from 350 to 540 m/s, at a depth range of 20–60 m. Below this sublayer lay a bedrock of high phase velocities from 560 to 680 m/s. The gentle slope of the original valley bed could be recognised from the results. Fig. 24 shows the SP variation along two survey lines near the upstream side (a–a′) and downstream side (b–b′). The SP profile at line a–a′ is indicative of a concentrated groundwater flowing on the right side and the absence of water-saturated zones on the left side and middle. The SP profile at line b–b′ showed negative SP anomalies, which should imply the presence of an infiltration of water flowing downward inside the dam material.

4.3. Terano landslide dam

Fig. 25 shows the topographic map of the Terano landslide dam in Niigata Prefecture, Japan. MTM surveys were performed in August 2014, 10 years after the landslide event, on survey lines TM–TM′–TM″

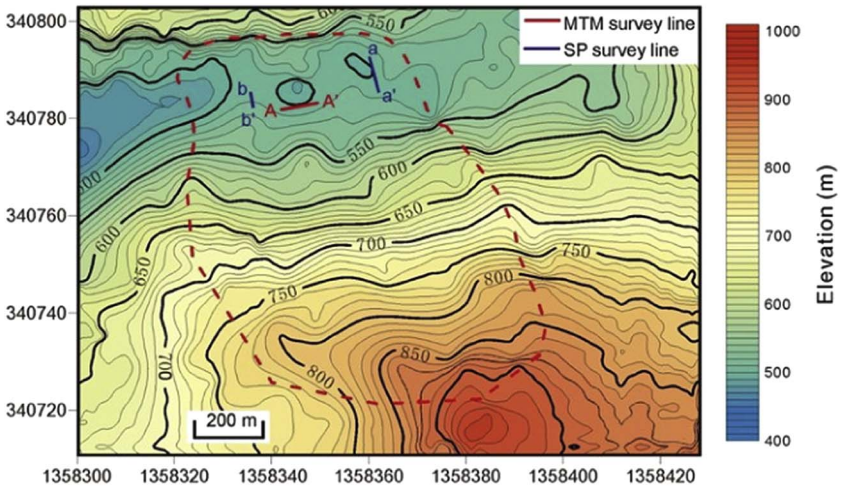

Fig. 19. Site map of the Kuridaira landslide dam indicating the survey lines for the microtremor (MTM) chain array and self-potential (SP) measurements. The dotted line indicates the boundary of the Kuridaira landslide.

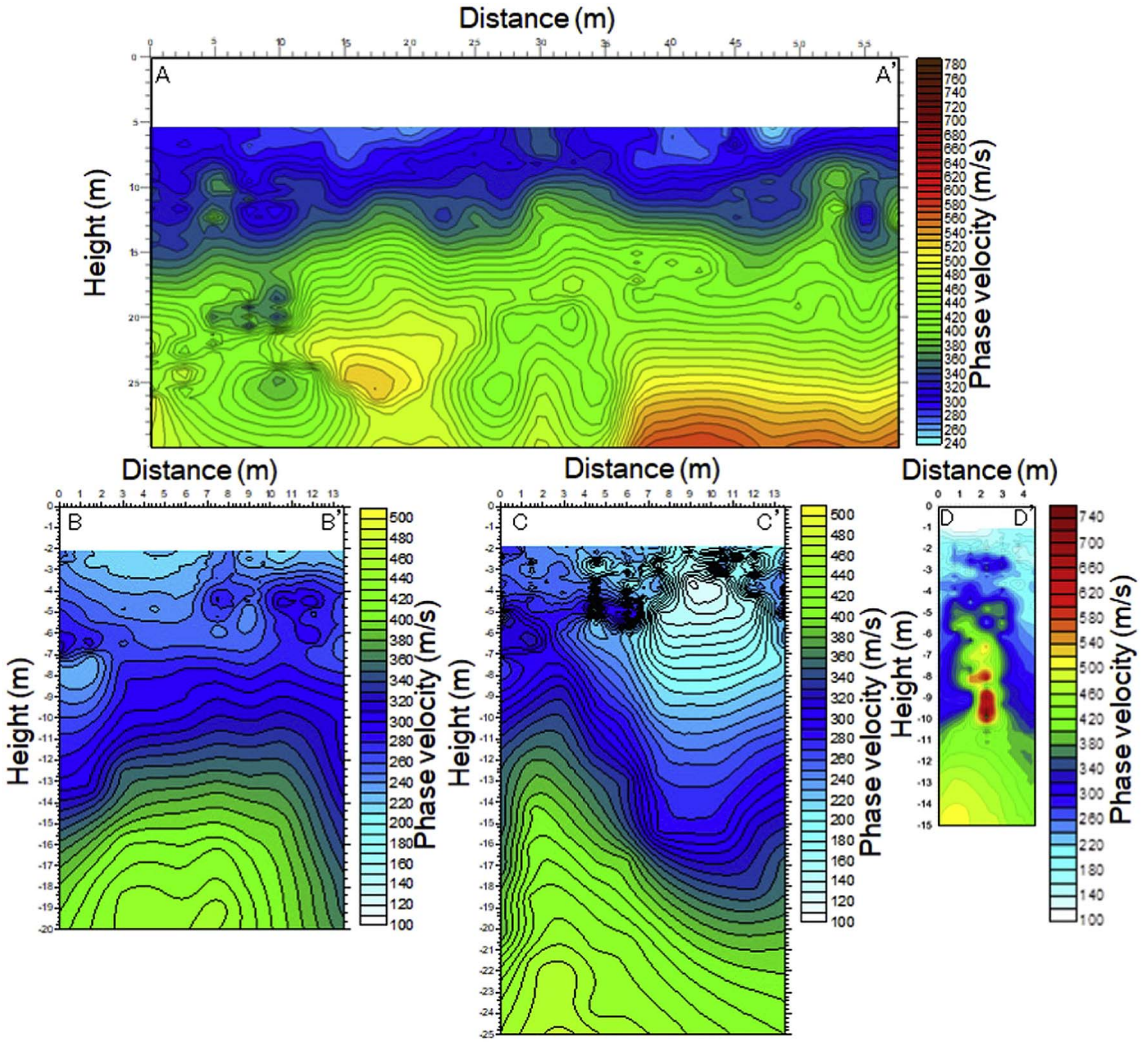

Fig. 20. Phase velocity versus depth profiles along survey lines A–A′, B–B′, C–C′ and D–D′ on the Akatani landslide dam. The same scale bar was used for all the profiles.

and CM–CM′. Here, TM″ and CM were at the same point. Moreover, SP surveys were carried out on survey lines CP–CP′ and LP–LP′. Here, lines CM–CM′ and CP–CP′ were set along the same position. The survey lines were chosen where there was a 3-m-wide road, and the longitudinal section of the landslide can be estimated from line TM–TM′–TM″. CP–CP′ and LP–LP′ were exactly parallel to the cross-section and longitudinal section of the landslide. Fig. 26 shows the phase velocity profile along the two surveyed lines. From the survey results, the phase velocity profile can be divided into three distinct layers. The upper layer had phase velocity ranging from 140 to 280 m/s, the middle

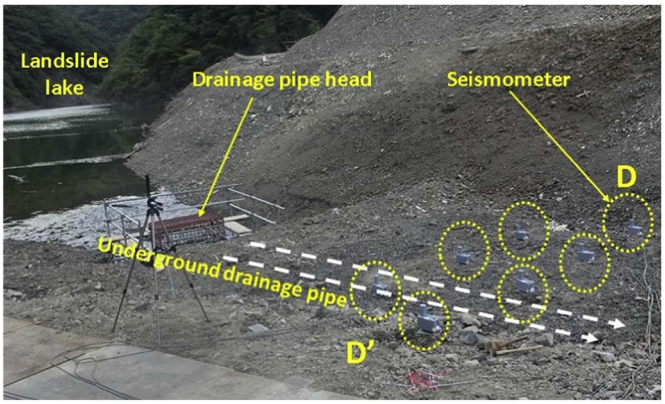

Fig. 21. The situation of survey line D–D′ on the upstream side of the Akatani landslide dam near the landslide lake. The drainage pipe head is visible. The path of the drainage pipe is indicated with dotted lines.

layer's phase velocity ranged from 280 to 360 m/s and the basal layer's phase velocity ranged from 360 to 480 m/s.

A previous study by Sassa (2005) approximated the angle of the sliding surface θ to be 20°, while the middle and basal layers of the landslide materials at line TM–TM′–TM″ dipped toward the landslide lake, with an inclination angle β of 13° (Fig. 26a). This lower inclination β may be because the profile direction is not parallel to the landslide direction, but instead, forms a 48° angle.

The results also showed the good performance of the MTM chain array survey in detecting the internal structure of the sliding mass on the sliding surface. Moreover, the discordant trends of phase velocities in the middle layer may suggest the effect of the impact force of the sliding mass on the valley floor, which could have modified the internal structure of the landslide dam (Fig. 26b).

Fig. 27 shows the SP profiles along survey lines CP–CP′ and LP–LP′. Points CP and LP were relatively high and dry. The negative SP anomalies in the order of 7–15 mV obtained at a horizontal distance of 4–28 m on line CP–CP′ could be attributed to an underground flow from the upper part of the landslide. Compared with the MTM chain array results, the loose structure in this area is deeper than that of the surrounding area (Fig. 27a). Similarly, a large negative SP anomaly of ~46 mV obtained at a horizontal distance of 68 m on the same survey line corresponded well to a shallow valley on the slope from the upper part of the landslide. The SP anomalies were predominantly positive (14–108 mV) on the left side of survey line LP–LP′, where there was a road, while the negative trend of the SP anomaly toward the right side of the survey line indicated a similar pattern of water flow as that

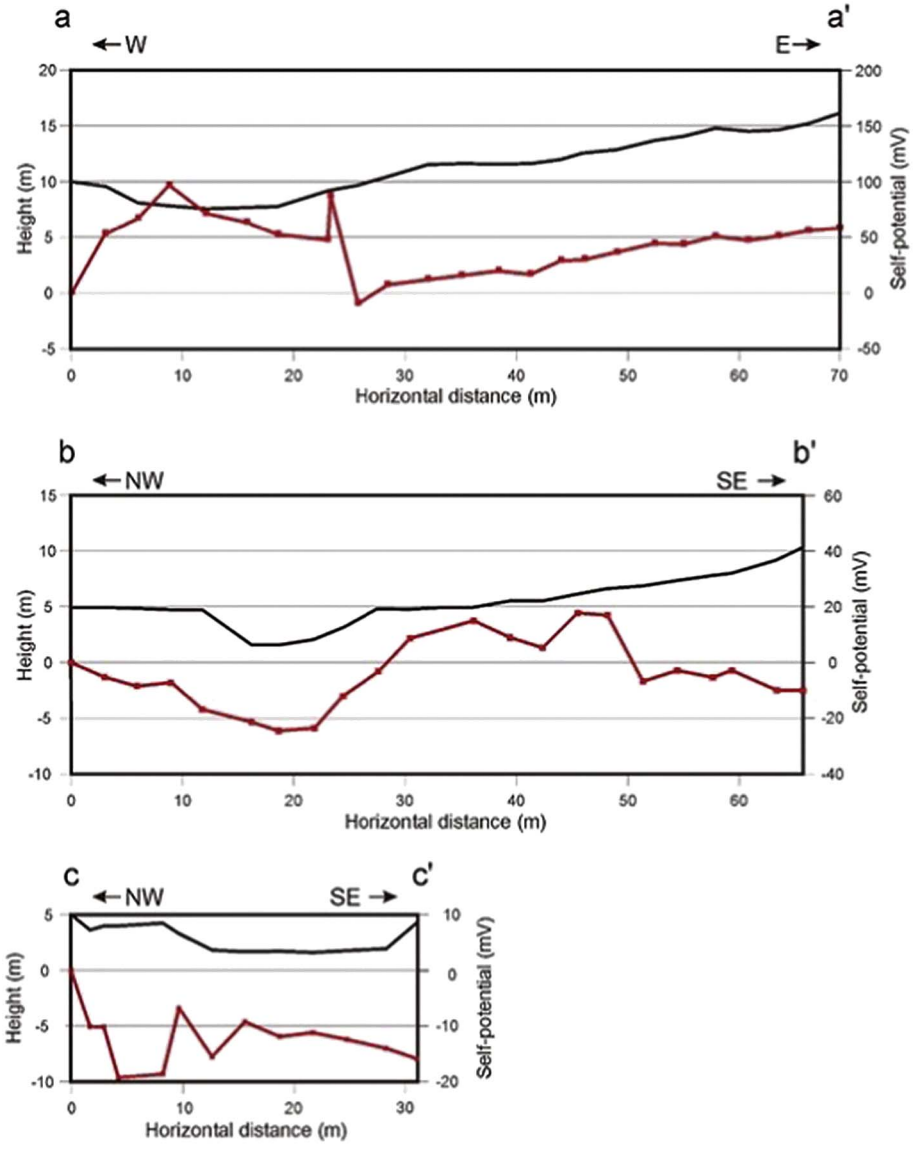

Fig. 22. Self-potential (SP) measurement profiles and results along lines a–a′, b–b′ and c–c′ at the Akatani landslide dam. The dotted lines are the measured SP values.

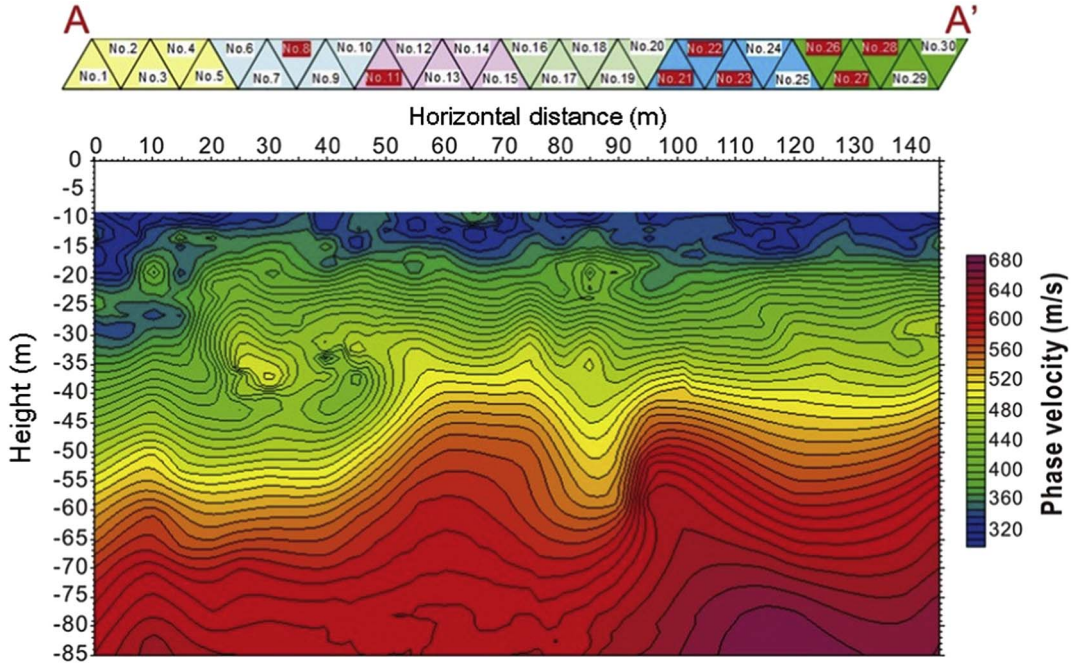

Fig. 23. Phase velocity versus depth profile along survey line A–A′ at the Kuridaira landslide dam.

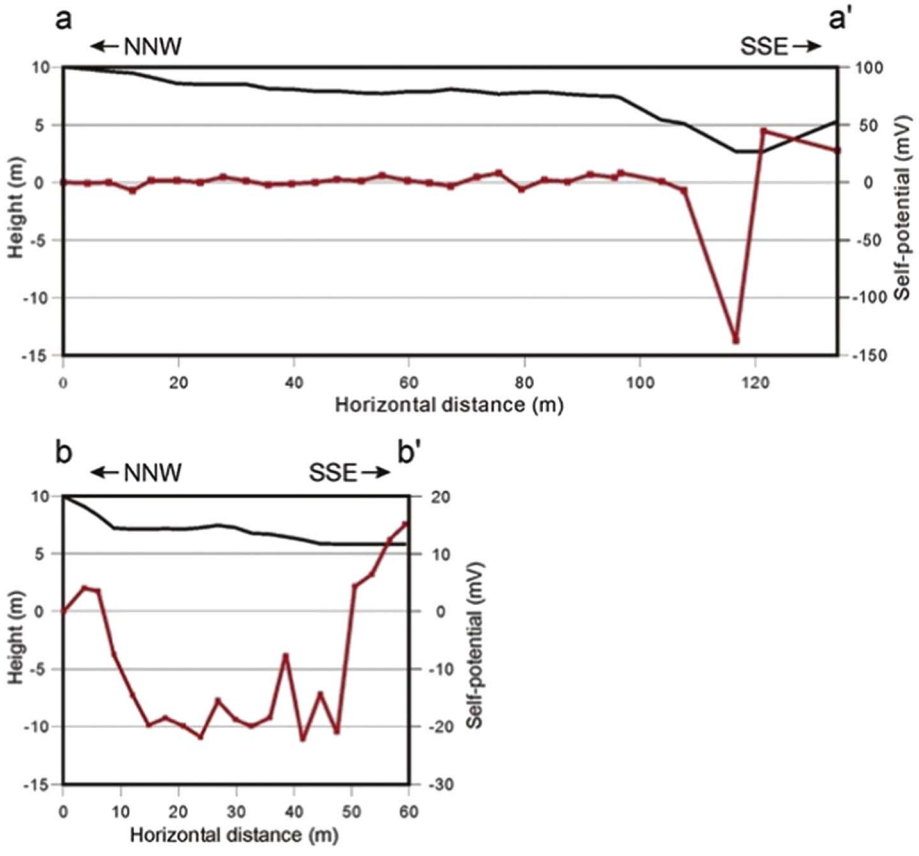

Fig. 24. Self-potential (SP) measurement profiles and results along lines a–a′ and b–b′ at the Kuridaira landslide dam. The dotted line is the measured SP.

shown on the right side of CP–CP′ (Fig. 27b).

At this site, although lines CM–CM′ and CP–CP′ were located at the same line, the results cannot be considered the effect of the flow inside the landslide dam, as there was one open channel in front of it, and the measured lines were completely parallel to the channel. However, it is also of interest that the negative SP value between 3 and 30 m in the CP–CP′ line corresponded to a loose structure at the same position of the CM–CM′ line. Ongoing seepage inside the landslide for about 10 years may have caused the loose structure.

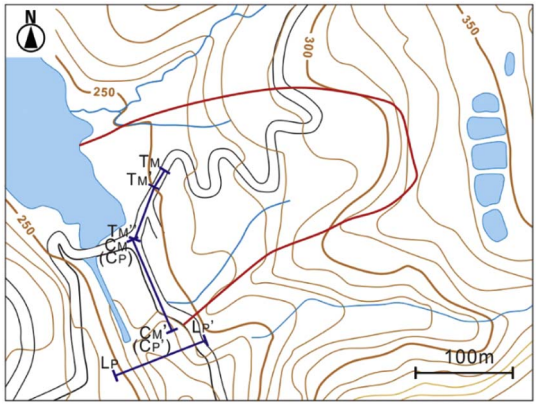

Fig. 25. Site map of the Terano landslide dam showing the survey lines for microtremor (MTM; TM–TM′–TM″ and CM–CM′) and self-potential (SP) measurements (CP–CP′ and LP–LP′).

4.4. Kol-Tor landslide dam

The map in Fig. 28 shows the measured line A–A′ from the MTM chain array and SP in the Kol-Tor landslide dam. The two types of measurement were conducted on the same line. The measure line was located at the toe part of the landslide dam and crossed the right boundary. The total length was 310 m.

Fig. 29 shows the Google Earth image of the same area shown in Fig. 28. In the middle of the landslide dam along the valley line, a concave topography can be observed, which may have been caused by the seeping from Kol-Tor Lake throughout the seasons for many years, sometimes the overflowing in summer. Near the toe part, seeping water and subsidence can even be observed on the Google Earth image.

Fig. 30 shows the results of the MTM chain array survey and SP survey at the toe of the Kol-Tor landslide dam. The array size for the MTM chain array survey and electrode spacing for the SP survey were both fixed at 10 m. The duration for each MTM chain array measurement was 30 min. The apparent phase velocity of the underlying debris varied from 240 to 760 m/s (Fig. 30a). The results showed marked variation in the phase velocity of the dam materials, including several concentrated zones of low phase velocity ranging from 240 to 280 m/s. This phenomenon could be attributed to the long-term seepage along the valley bed, and the position corresponded well to the exit point of the seepage water from the landslide dam. The low phase velocity of 240–460 m/s that dominated the upper half of the landslide dam can be ascribed to the moderately consolidated nature of the sediments, comprising clast-supported and inversely graded materials of high hydraulic conductivity. Similarly, the marked variation in the phase velocity of the upper layer may suggest the prolonged effects of seasonal glacier-ice melt, torrential rainfall and occasional rise in the upstream lake level, leading to occasional overflow of the lake waters. The underlying layer was characterised by asymmetrical zones of high phase velocities (460–760 m/s), dipping rightward (toward the upstream lake) with an inclination of 28–35° and leftward (toward the downstream slope) with an inclination of 18–55°. The highly consolidated nature of the glaciogenic sediments may have contributed to the high phase velocity of this layer. Fig. 30b shows the SP profile along the survey line. The measurement was initiated on a gentle slope, so the base station was relatively high and dry. The results indicate that the left side of the survey line (0–180 m) was dominated by negative SP anomalies varying in the range of 4–22 mV, which corresponded well to the area of the landslide dam; the right side was dominated by positive SP anomalies varying in the range of 10–46 mV, which corresponded well to a debris flow deposit in the dry climate of the high mountains. This trend is consistent with the hydrological regime of the surrounding catchment basin. Apart from an active seepage zone that corresponded to a horizontal distance of 150 m, a few other seepage exit points were observed at the downstream slope at horizontal distances of 80 m and

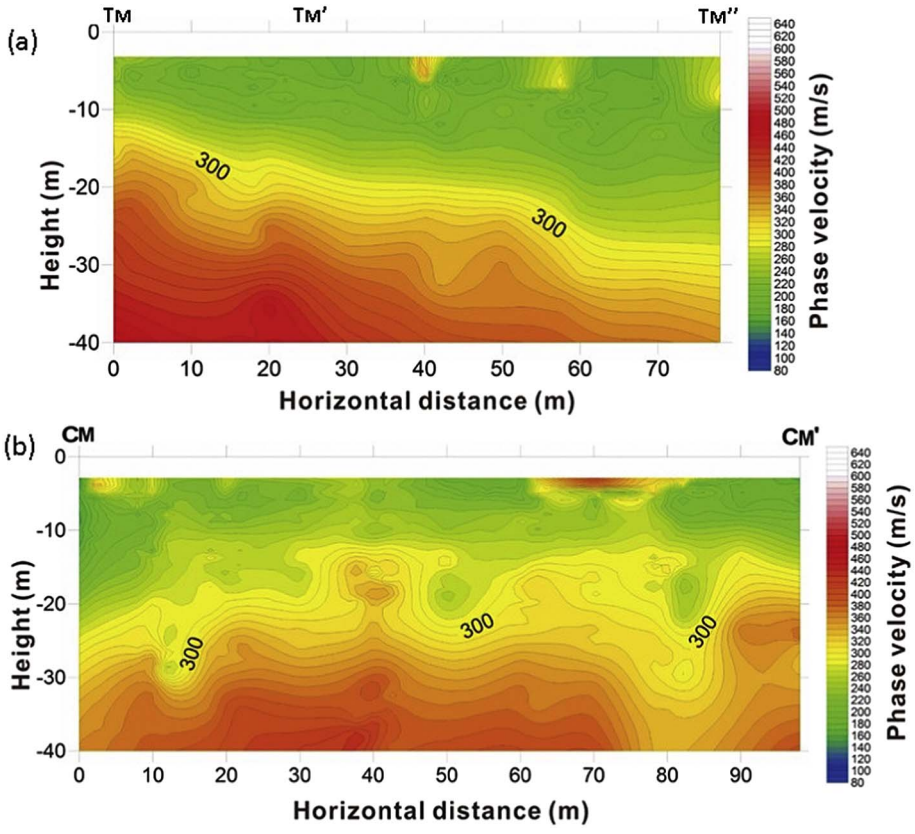

Fig. 26. Phase velocity versus depth profiles of the Terano landslide dam along the microtremor (MTM) chain array measurement: a) line TM–TM′–TM″, b) line CM–CM′.

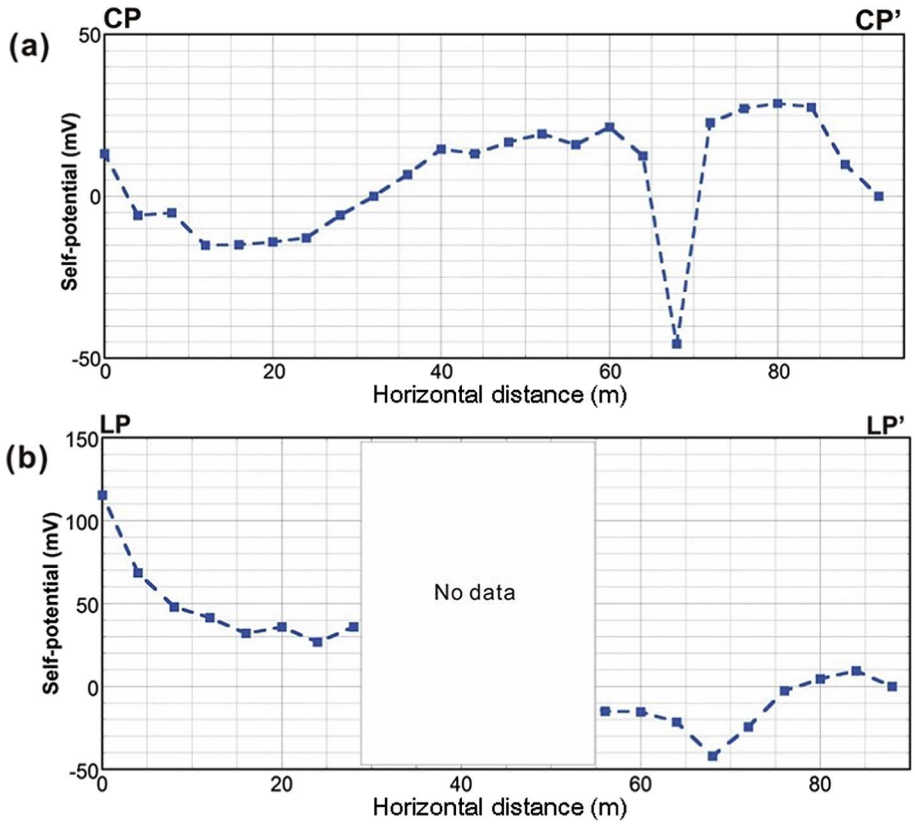

Fig. 27. Self-potential (SP) measurement results on the Terano landslide dam: a) line CP–CP′, b) line LP–LP′.

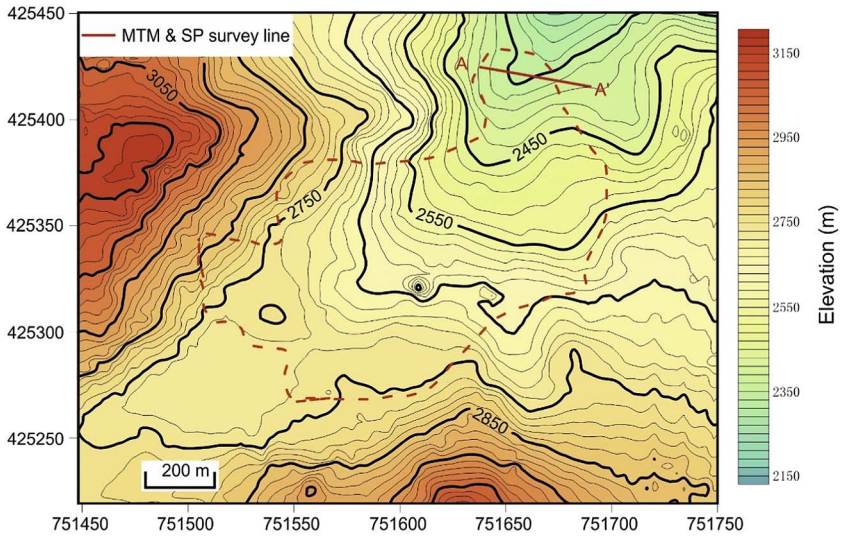

Fig. 28. Site map of the Kol-Tor landslide dam indicating the microtremor (MTM) chain array and self-potential (SP) survey lines. The dotted line indicates the boundary of the landslide dam.

170 m. The horizontal distance of 220 m was almost the right boundary of the landslide dam.

Through this investigation, it was found that the seepage route can be detected well by SP survey. Moreover, the situation of the internal erosion that has occurred inside the landslide dam can be evaluated using an MTM chain survey.

Integrating the results of the MTM chain and SP surveys, it is interesting to find that the negative SP values between 0 and 150 m corresponded well with the downstream side of the landslide dam, which can be recognised not only from the topography, but also the MTM chain survey. For this long-existing landslide dam, which has been subject to seepage and internal erosion for hundreds of years, the integration of the two methods can reveal the internal structure well and show the area where groundwater is flowing.

5. Conclusions

This research demonstrated the applicability of geophysics to the investigation and evaluation of the current internal structure of landslide dams and possible groundwater flow routes inside them. An integrated geophysical approach comprising MTM chain array and SP surveys was successfully employed to delineate zones eroded by piping and determine the seepage routes in landslide dams.

The methods have high potential for the evaluation of landslide dams' internal structures and detection of the piping routes in landslide dams three-dimensionally when multiple parallel measure lines cross

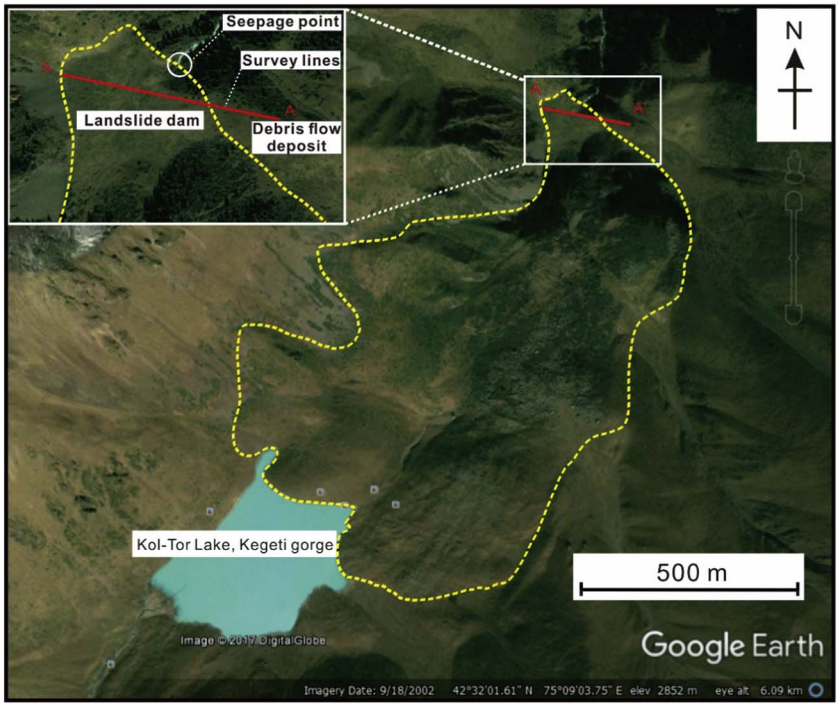

Fig. 29. Situation of the Kol-Tor landslide dam and the location of the survey line on the Google Earth image. The dotted line indicates the boundary of the landslide dam.

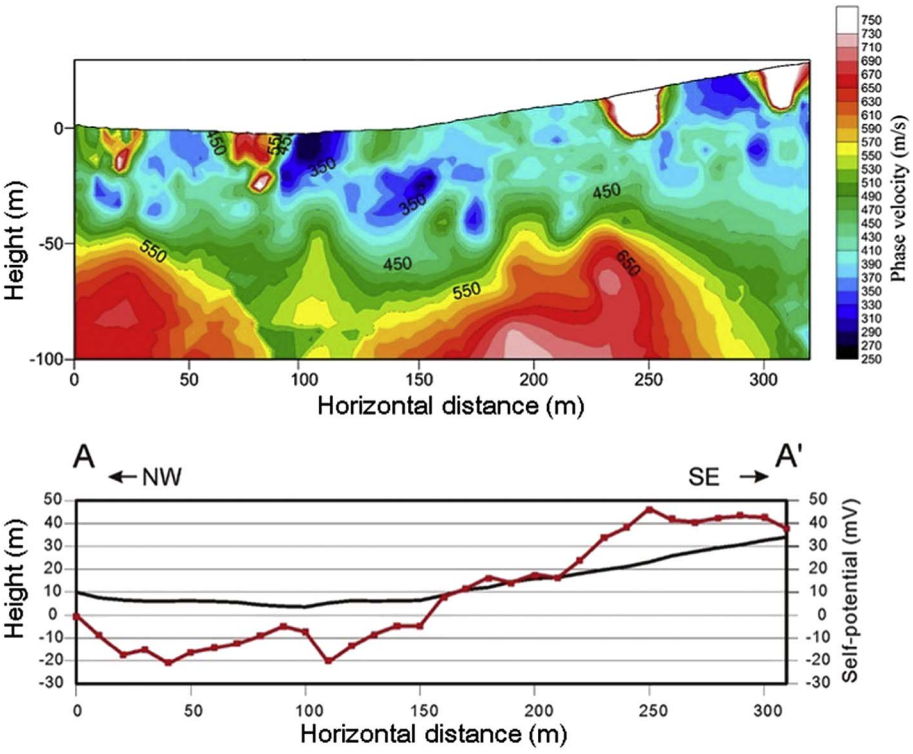

Fig. 30. Microtremor (MTM) chain array and self-potential (SP) measurement results for the Kol-Tor landslide dam: a) Phase velocity versus depth profile, b) measure line topography (black line) and SP profile (red line with dots). (For interpretation of the references to colour in this figure legend, the reader is referred to the web version of this article.)

the potential flow direction of the underground water. The results will be important not only for the failure prediction of landslide dams, but also for countermeasure works, such as those to reinforce these dams.

Acknowledgements

This work was supported by a JSPS KAKENHI grant (Number A-2424106) for landslide dam failure prediction and Shimane University grant (Juten-2017-2019) for natural disaster reduction study. Prof. Hideaki Marui of Niigata University joined the field investigation at the Terano landslide dam. Dr. Isakbek Torgoev, Director of the 'GEOPRIBOR' Scientific-Engineering Centre, National Academy of Sciences of the Kyrgyzstan Republic, and his colleagues helped us in the field investigations at the Kol-Tor landslide dam. Mr. Y. Mitani, Mr. Y. Kuwada, Mr. M. Hoshimoto, Mr. R. Shinmitsu, Mr. F. Faris and Mr. H.F. Yang joined the field investigation. Mr. S. Zhang drew some maps and figures. The comments from the two reviewers were extremely helpful in improving the quality of this paper.

References

Aki, K., 1957. Space and time spectra of stationary stochastic waves, with special reference to microtremors. Bull Earthq. Res. Inst. 35, 415–456.

Aki, K., 1965. A note on the use of microseisms in determining the shallow structures of the earth's crust. Geophysics 30 (4), 665–666.

Allegre, V., Jouniaux, L., Lehmann, F., Sailhac, P., 2010. Streaming potential dependence on water-content in Fontainebleau sand. Geophys. J. Int. 182 (3), 1248–1266.

Apostolidis, P.I., Raptakis, D.G., Roumelioti, Z., Pitilakis, K.D., 2004. Determination of S-wave velocity structure using microtremors and SPAC method applied in Thessaloniki (Greece). Soil Dyn. Earthq. Eng. 24 (1), 49–67.

Apostolidis, P.I., Raptakis, D.G., Pandi, K.K., Manakou, M.V., Pitilakis, K.D., 2006. Definition of subsoil structure and preliminary ground response in Aigion city (Greece) using microtremor and earthquakes. Soil Dyn. Earthq. Eng. 26 (10), 922–940.

Arai, H., Tokimatsu, K., 2004. S-wave velocity profiling by inversion of microtremor H/V spectrum. Bull. Seismol. Soc. Am. 94 (1), 53–63.

Asten, M.W., 2004. Passive seismic methods using the microtremor wave field for engineering and earthquake site zonation. In: Proceedings of the SEG 74th Annual Meeting.

Asten, M.W., Stephenson, W.R., Davenport, P.N., 2005. Shear-wave velocity profile for Holocene sediments measured from microtremor array studies, SCPT, and seismic refraction. J. Environ. Eng. Geophys. 10 (3), 235–242.

Becker, J.S., Johnston, D.M., Paton, D., Hancox, G.T., Davies, T.R., McSaveney, M.J., Manville, V.R., 2007. Response to landslide dam failure emergencies: issues resulting from the October 1999 Mount Adams landslide and dam-break flood in the Poerua River, Westland, New Zealand. Nat. Hazards Rev. 8 (2), 35–42.

Bolève, A., Revil, A., Janod, F., Mattiuzzo, J.L., Fry, J.J., 2009. Preferential fluid flow pathways in embankment dams imaged by self-potential tomography. Near Surf. Geophysics 7 (5–6), 447–462.

Brown, L.T., Diehl, J.G., Nigbor, R.L., 2000. A simplified procedure to measure average shear-wave velocity to a depth of 30 meters (VS30). In: Proceedings of 12th World Conference on Earthquake Engineering.

Capon, J., 1969. High-resolution frequency-wavenumber spectrum analysis. Proc. IEEE 57, 1408–1418.

Corwin, R.F., 1990. The self-potential method for environmental and engineering applications. Geotechnical and environmental. Geophysics 1, 127–145.

Corwin, R.F., 1991. Evaluation of effects of cutoff wall construction on seepage flow using self-potential data, east embankment Wells dam. In: Report for Douglas County Public Utility District No. 1, Washington.

Costa, J.E., Schuster, R.L., 1988. The formation and failure of natural dams. Geol. Soc. Am. Bull. 100 (7), 1054–1068.

Dong, J.J., Tung, Y.H., Chen, C.C., Liao, J.J., Pan, Y.W., 2009. Discriminant analysis of the geomorphic characteristics and stability of landslide dams. Geomorphology 110 (3), 162–171.

Ermini, L., Casagli, N., 2003. Prediction of the behaviour of landslide dams using a geomorphological dimensionless index. Earth Surf. Process. Landf. 28 (1), 31–47.

Evans, D.G., 1986. The maximum discharge of outburst floods caused by the breaching of man-made and natural dams. Can. Geotech. J. 23 (3), 385–387.

Evans, S.G., Delaney, K.B., Hermanns, R.L., Strom, A., Scarascia-Mugnozza, G., 2011. The formation and behaviour of natural and artificial rockslide dams; implications for engineering performance and hazard management. In: Evans, Hermanns, Strom, Scarascia-Mugnozza (Eds.), Natural and Artificial Rockslide Dams. Springer, Berlin Heidelberg, pp. 1–75.

García-Jerez, A., Luzón, F., Navarro, M., Pérez-Ruiz, J.A., 2008. Determination of elastic properties of shallow sedimentary deposits applying a spatial autocorrelation method. Geomorphology 93 (1), 74–88.

Glover, P.W., Walker, E., Jackson, M.D., 2012. Streaming-potential coefficient of reservoir rock: a theoretical model. Geophysics 77 (2), D17–D43.

Hayashi, S., Matsuoka, T., Mizuochi, Y., Ono, M., 2010. Two dimensional microtremors survey – chain array survey method. Geotech. Eng. Mag. 58 (8), 10–13.

Hayashi, S., Uchida, T., Okamoto, A., Ishizuka, T., Yamakoshi, T., Morita, K., 2013. Countermeasures against landslide dams caused by Typhoon talas 2011. Tech. Monitor 20–26.

Ibs-von Seht, M., Wohlenberg, J., 1999. Microtremor measurements used to map thickness of soft sediments. Bull. Seismol. Soc. Am. 89 (1), 250–259.

Ishido, T., Mizutani, H., Baba, K., 1983. Streaming potential observations, using geothermal wells and in situ electrokinetic coupling coefficients under high temperature. Tectonophysics 91 (1), 89–104.

Janský, B., Šobr, M., Engel, Z., 2010. Outburst flood hazard: case studies from the Tien-Shan Mountains, Kyrgyzstan. Limnologica-Ecol. Manag. Inland Waters 40 (4), 358–364.

Jouniaux, L., Ishido, T., 2012. Electrokinetics in earth sciences: a tutorial. Int. J. Geophys. 2012. http://dx.doi.org/10.1155/2012/286107.

King, J., Loveday, I., Schuster, R.L., 1989. The 1985 Bairaman landslide dam and resulting debris flow, Papua New Guinea. Q. J. Eng. Geol. Hydrogeol. 22 (4), 257–270.

Korup, O., 2004. Geomorphometric characteristics of New Zealand landslide dams. Eng. Geol. 73 (1), 13–35.

Korup, O., McSaveney, M.J., Davies, T.R., 2004. Sediment generation and delivery from large historic landslides in the Southern Alps, New Zealand. Geomorphology 61 (1), 189–207.

Lacoss, R.T., Kelly, E.J., Toksoz, M.N., 1969. Estimation of seismic noise structure using arrays. Geopgysics 34, 21–38.

Ling, S., Okada, H., 1993. An extended use of the spatial autocorrelation method for the estimation of geological structure using microtremors. In: Proc of the 89th SEGJ Conference, pp. 44–48 (in Japanese).

Lowrie, W., 2007. Fundamentals of Geophysics. Cambridge University Press (354 p).

Matsuoka, T., Umezawa, N., Makishima, H., 1996. Experimental studies on the applicability of the spatial autocorrelation method for estimation of geological structures using microtremors. Butsuri-Tansa 49 (1), 26–41 (in Japanese with English abstract).

Moore, J.R., Boleve, A., Sanders, J.W., Glaser, S.D., 2011. Self-potential investigation of moraine dam seepage. J. Appl. Geophys. 74 (4), 277–286.

Nagai, Y., Maruyama, J., Yoshida, K., Yamakoshi, T., 2008. Emergency response and permanent measures for large landslide dams triggered by the 2004 Mid-Niigata Prefecture Earthquake in Japan. Int. J. Erosion Control Eng. 1 (1), 20–29.

Nakamura, Y., 1989. A method for dynamic characteristics estimation of subsurface using microtremor on the ground surface. Railway Tech. Res. Inst. Q. Rep. 30 (1).

Ohori, M., Nobata, A., Wakamatsu, K., 2002. A comparison of ESAC and FK methods of estimating phase velocity using arbitrarily shaped microtremor arrays. Bull. Seismol. Soc. Am. 92 (6), 2323–2332.

Okada, H., 1994. A research on the practical application of microtremor exploration techniques to a wide area survey of a underground structure under 3,000 m in depth. In: Report of a Grant-in0Aidfor Co-operative Research (B) No.03554009 Supported by the Scientific Research Fund in 1993, (in Japanese).

Okada, H., 2001. Consideration about the effective observation point number in the space autocorrelation method for microtremor array survey. In: Proc. of 104th SEGJ Conference, pp. 26–30 (in Japanese).

Okada, H., 2003. The Microseismic Survey Method: Society of Exploration Geophysicists of Japan. Translated by Koya Suto. Geophysical Monograph Series. pp. 12.

Okada, H., 2006. Theory of efficient array observations of microtremors with special reference to the SAC method. Butsuri-Tansa 59, 73–85.

Okada, H., Matsushima, T., Moriya, T., Sasatani, T., 1990. An exploration technique using long-period microtremors for determination of deep geological structures under urbanized areas. Butsuri-Tansa 43 (6), 402–417 (in Japanese with English abstract).

Okada, H., Matsuoka, T., Shiraishi, H., Hachinohe, S., 2003. Spatial autocorrelation algorithm for the microtremor survey method using semicircular arrays. In: Proc. of 109th SEGJ Conference, pp. 183–196 (in Japanese).

Roberts, J.C., Asten, M.W., 2005. Estimating the shear velocity profile of Quaternary silts using microtremor array (SPAC) measurements. Explor. Geophys. 36 (1), 34–40.

SABO (Erosion and sediment control) Division of the Water and Disaster Management Bureau, the Ministry of Land, Infrastructure, Transport and Tourism, and the Public Works Research Institute, 2012. Press Release Dated September 10, 2012, on Surveys on Deep Catastrophic Landslides at the Stream (Small Watershed) Level. *http://www.mlit.go.jp/report/press/mizukokudo03_hh_000552.html* (in Japanese).

Sakurai, W., Sakai, R., Okuyama, Y., Mizuyama, T., Ikeda, A., Kaihara, S., Tadakuma, N., Kashiwabara, Y., Yoshino, K., Ogawauchi, Y., Tatsumi, H., 2016. Large-scale erosion and sediment discharge at landslide dams and issues with countermeasures during Typhoon No. 11 (Halong) on August 10, 2014. J. Jpn. Soc. Erosion Control. Eng. 68 (6).

Sasaki, T., Hayashi, H., Tanase, A., Harayama, S., Mizuochi, Y., Minami, Y., 2015. The S-wave velocity structure and the phase velocity distribution by the microtremor array survey. In: Proceedings of the 10th Asian Regional Conference of IAEG, Kyoto, Japan.

Sassa, K., 2005. Landslide disasters triggered by the 2004 Mid-Niigata Prefecture earthquake in Japan. Landslides 2 (2), 135–142.

Satofuka, Y., Mori, T., Mizuyama, T., Ogawa, K., Yoshino, K., 2010. Prediction of floods caused by landslide dam collapse. J. Disaster Res. 5 (3), 288–295.

Satoh, T., Kawase, H., Matsushima, S.I., 2001. Estimation of S-wave velocity structures in and around the Sendai Basin, Japan, using array records of microtremors. Bull. Seismol. Soc. Am. 91 (2), 206–218.

Schuster, R.L., Wieczorek, G.F., Hope, D.G., 1998. Landslide dams in Santa Cruz County, California, resulting from the earthquake. US Geol. Surv. Prof. Pap. 1551C.

Sjödahl, P., Dahlin, T., Johansson, S., 2005. Using resistivity measurements for dam safety evaluation at Enemossen tailings dam in southern Sweden. Environ. Geol. 49 (2), 267–273.

Thompson, S., Kulessa, B., Luckman, A., 2012. Integrated electrical resistivity tomography (ERT) and self-potential (SP) techniques for assessing hydrological processes within glacial lake moraine dams. J. Glaciol. 58 (211), 849–858.

Walder, J.S., O'Connor, J.E., 1997. Methods for predicting peak discharge of floods caused by failure of natural and constructed earthen dams. Water Resour. Res. 33 (10), 2337–2348.